Supporting Information: Rydberg Electron Stabilizes the Charge Localized State of the Diamine Cation

Marc Reimann,[†] Christoph Kirsch,[‡] Daniel Sebastiani,[‡] and Martin Kaupp[*,†]

†*Theoretische Chemie/Quantenchemie, Institut für Chemie, Technische Universität Berlin, 10623 Berlin, Germany.*

‡*Institut für Chemie, Martin-Luther-University Halle-Wittenberg, 06120 Halle (Saale), Germany*

E-mail: martin.kaupp@tu-berlin.de

1 Performance of Single-Reference Wave-Function Methods for DMP$^+$

To address the performance of the gold standard CCSD(T) of single-reference wave-function methods along the BHandHLYP-generated reaction path (see Computational Details in main text), we performed single-point calculations at the UHF-UCCSD(T)/aug-cc-pVDZ level of theory, which is very close to the methodology employed in Ref S1. When inspecting Mulliken spin populations of the resulting UHF wave functions we realized that not one unique, but three qualitatively different UHF-solutions could be found along the path: one in which the positive charge localizes at that nitrogen atom where it also localizes at BHandHLYP level (solution A), one where it is localized at the other nitrogen atom (solution B), and a delocalized solution (solution C) (Figure S1).

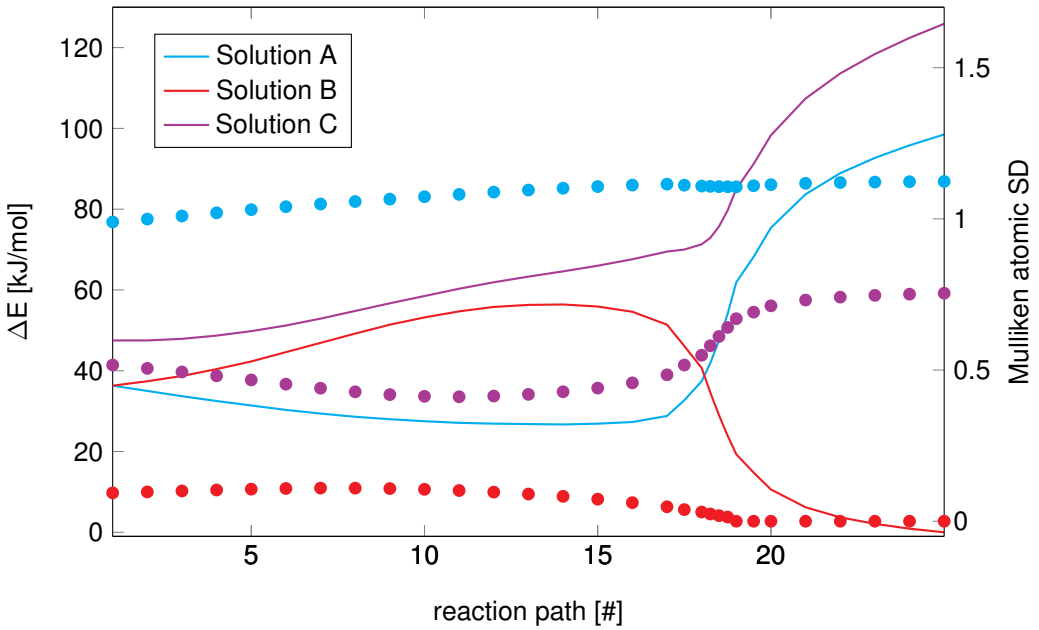

Figure S1: Energies in kJ/mol of three different UHF/aug-cc-pVDZ solutions obtained along the BHandHLYP-generated DMP-D$^+$→DMP-L$^+$ pathway, given relative to the lowest-energy point for solution B (lines, left axis scale). Dots give Mulliken atomic spin densities for the same three solutions at that nitrogen atom, where the positive charge is localized for the BHandHLYP DMP-L$^+$ calculation (right axis scale).

The three UHF solutions show different, unexpected behaviors. The charge-delocalized

solution C, which might be expected to be qualitatively correct at the DMP-D$^+$ minimum, gives the highest UHF energy at that point. The minimum of the charge-localized solution A, which should be correct at the DMP-L$^+$ minimum, lies close to the midpoint of the path, while the overall lowest energy is provided by the chemically non-intuitive solution B. Solution B is also the only solution that shows a barrier along the reaction path, while it erroneously features DMP-L$^+$ as the lower-energy minimum. Neither A nor C exhibit barriers along the path. The overall minimum-energy path does exhibit a barrier, but this arises exclusively from the unphysical crossing from A to B near point 18.

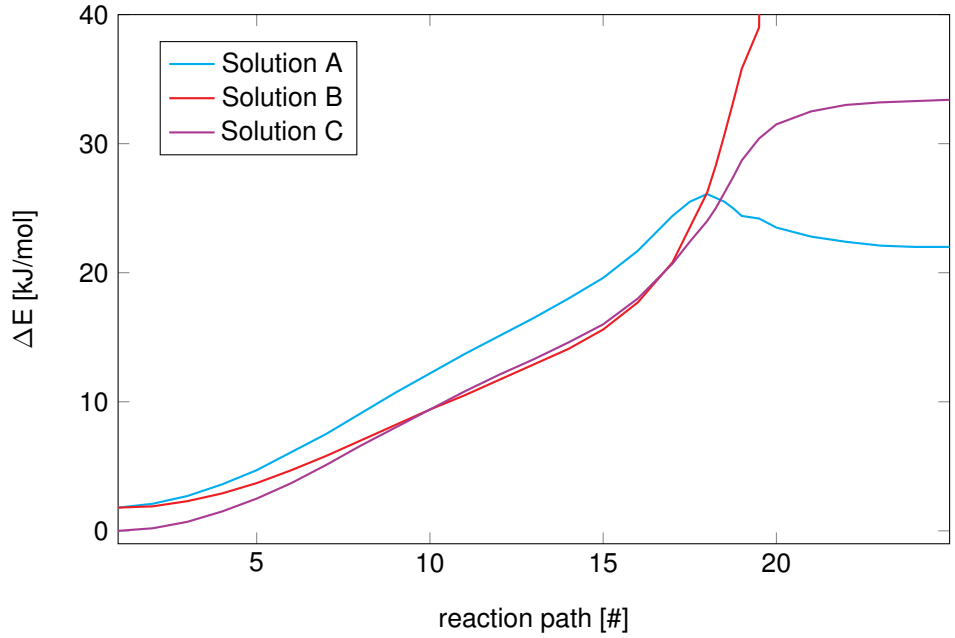

Figure S2: CCSD/aug-cc-pVDZ energies in kJ/mol based on the three different UHF/aug-cc-pVDZ solutions obtained along the BHandHLYP-generated DMP-D$^+$→DMP-L$^+$ pathway, given relative to the lowest-energy point for solution C.

CCSD wavefunctions obtained with these UHF references compensate this unphysical behavior mostly but not completely. Solution C correctly gives the lowest CCSD energy at the DMP-D$^+$ structure (Figure S2, left), while the UHF solution was above the other solutions (see above). We may view this as an example of Löwdin's dilemma of post-Hartee-Fock methods.[S2] The qualitatively wrong UHF curve of solution B is also cured at the CCSD level. In agreement with chemical intuition, it now gives very high energies in the DMP-L$^+$

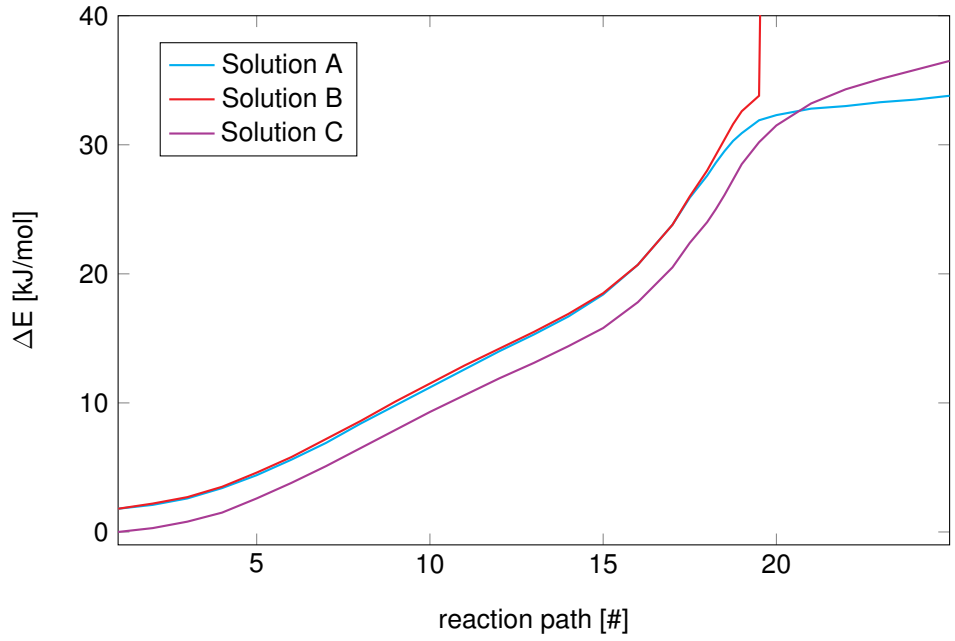

Figure S3: CCSD(T)/aug-cc-pVDZ energies in kJ/mol based on the three different UHF/aug-cc-pVDZ solutions obtained along the BHandHLYP-generated DMP-D$^+$→DMP-L$^+$ pathway, given relative to the lowest-energy point for solution C.

region, more than 100 kJ/mol above those obtained from the other solutions. The small maximum (4 kJ/mol above the "DMP-L$^+$ region") in the curve based on solution A exists in exactly the area where UHF solutions A and B cross (cf. Figure S1). The curves based on UHF solutions B and C change only marginally when perturbative triple substitutions are included at CCSD(T) level (Figure S3). The small local maximum that curve A exhibited at CCSD level is eliminated by the triple contributions. CCSD D_1 diagnostics (Figure S4) indicate problems for curve B in the "DMP-L$^+$ region" (and large values for curve C further to the right) and a crossing between the D_1 curves A and B near the CCSD "barrier". While this suggests a potential importance of perturbational triples contributions,[S3] borne out by the energy curves (see above), the values are no reliable indicators of multi-reference character. A number of authors, e.g. Jiang et al.,[S4] have suggested the use of a combined set of different types of diagnostics to assess the quality of CCSD wave functions in the case of 3d transition-metal species. Our calculated contributions of the (T) corrections to the total atomization energies (%TAE$_e$[(T)]), for example, are all in the range 1.3–1.5 %, independent

of the UHF reference function chosen and well below the commonly considered threshold of 10 %.[S4]

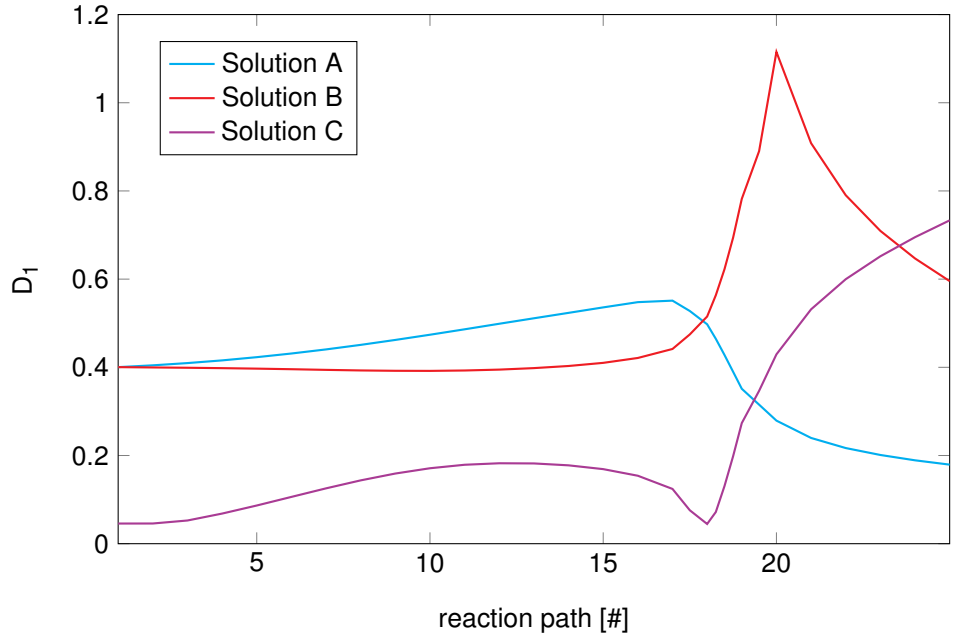

Figure S4: D1 diagnostics of the CCSD/aug-cc-pVDZ wave functions based on the three different UHF/aug-cc-pVDZ solutions along the BHandHLYP-generated DMP-D$^+$→DMP-L$^+$ pathway. See Fig. S3 for the corresponding energies.

The above discussion indicates that the coupled-cluster energy curves reflect to some extent artefacts arising from the presence of multiple UHF solutions with widely varying behavior along the potential "reaction path". Different remedies are available in such cases. When using a generalized Kohn-Sham (GKS) instead of a UHF reference wave function, symmetry breaking can be reduced by the implicit inclusion of electron correlation in the reference orbitals. This reduces single-excitation contributions, leading to lower D_1 values. GKS-CCSD and GKS-CCSD(T) results based on BHandHLYP orbitals are shown in Figure S5. As was true for UHF solution A (see above), the CCSD surface shows a small barrier that vanishes upon inclusion of the (T) correction. Unlike the UHF solution, however, the maximum D_1 value along the surface is now 0.08, significantly below those obtained for the HF solution and below critical thresholds. Use of Brueckner orbitals,[S5–S7] where the D_1 diagnostic vanishes by construction, gives almost identical energy curves. The bias

from a specific open-shell reference can be circumvented altogether by employing the IP-EOM-CCSD procedure[S8] on a closed-shell reference. This approach has been used before to circumvent symmetry breaking of the reference wave function.[S9] As the IP-EOM-CCSD energy curve is almost identical to the one obtained at BCCD(T) and GKS-CCSD(T) levels (Figure S5), we strongly suspect that the small barriers seen at CCSD levels indeed arise from artificial symmetry breaking of the open-shell reference wave function, while the (T) corrections are physically justified, and the CCSD(T) calculations may be considered to exhibit the correct behavior.

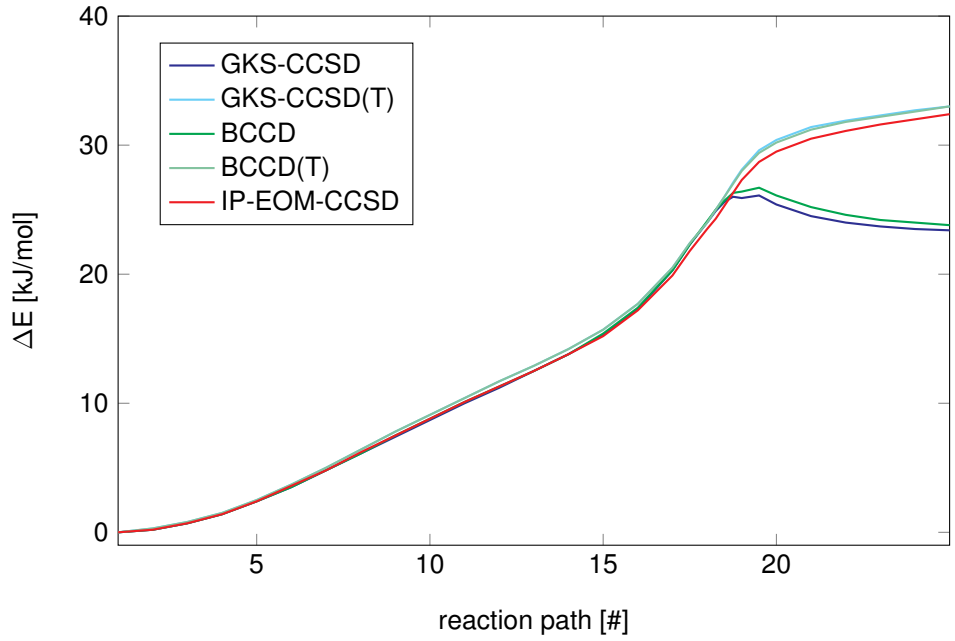

Figure S5: Energy curves in kJ/mol (relative to the lowest energy at a given level) along the BHandHLYP-generated DMP-D$^+$→DMP-L$^+$ pathway obtained at GKS-CC levels (with BHandHLYP orbitals), Brückner-CC levels, as well as with IP-EOM-CCSD. aug-cc-pVDZ results.

In the context of UHF artefacts generating an artificial barrier, we also scanned the "reaction path" with functionals where the EXX admixture of BHandHLYP-type functionals is varied systematically between 0 % and 100 % in steps of 10 %. The energy curves are compared in Figure S6. A barrier is generated when reaching an EXX admixture of 50 % – just the amount present in BHandHLYP – suggesting that the functional inherits the

unphysical symmetry breaking of the UHF solutions. Possibly the semi-local terms in more highly parameterized functionals like M06-HF can to some extent counteract the large UHF contributions and remove the artificial barrier.

Interestingly, we also find no barrier when we use the three different UHF states as a basis for a non-orthogonal configuration interaction (NOCI) treatment,[S10] which results in more physically correct states that, for example, avoid crossings.[S11] At this level, the qualitatively wrong preference of UHF for DMP-L$^+$ is also cured (Figure S7). Such a treatment has been shown before to be applicable to related electron-transfer problems.[S12]

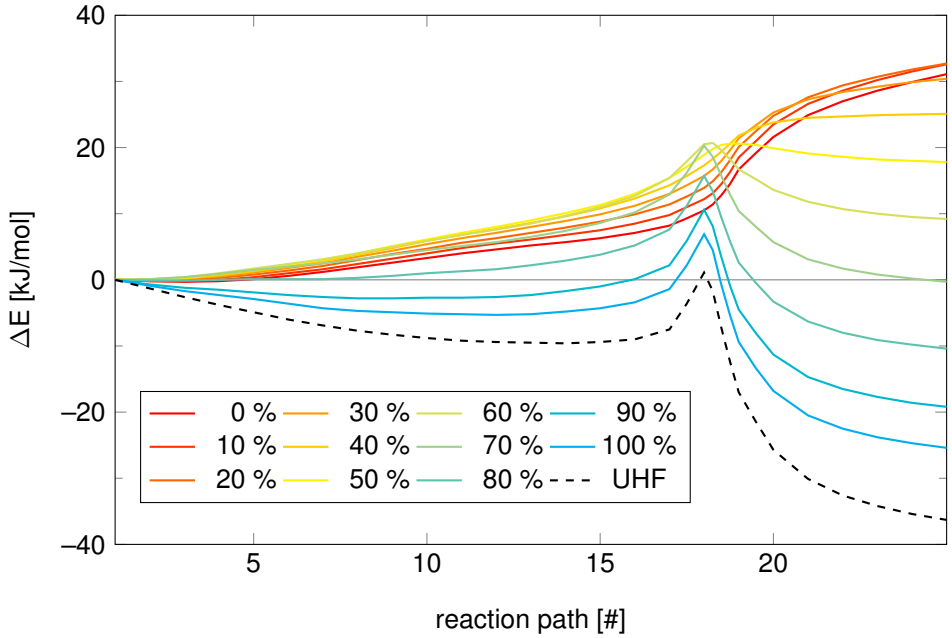

Figure S6: Energy curves in kJ/mol (relative to the DMP-D$^+$ minimum) along the BHandHLYP-generated DMP-D$^+$→DMP-L$^+$ pathway obtained with B1LYP-type functionals from 0% EXX admixture (BLYP, red) to 100% (cyan) in steps of 10%. The corresponding UHF curve is shown for comparison (black dashes). aug-cc-pVDZ results.

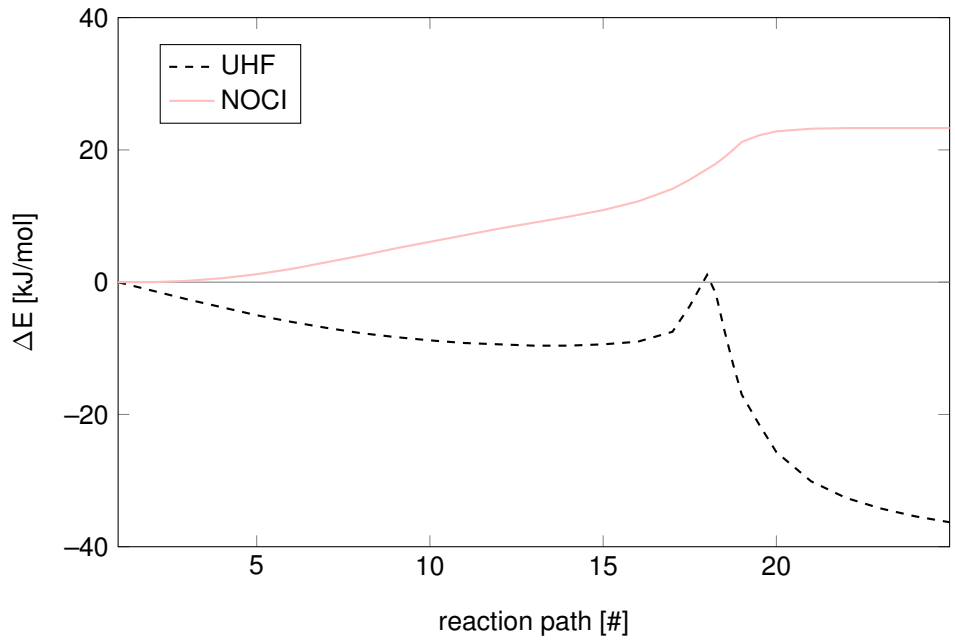

Figure S7: Three-determinant non-orthogonal CI energy curve (see text) compared to UHF curve (in kJ/mol) along the BHandHLYP-generated DMP-D$^+$→DMP-L$^+$ pathway, relative to the DMP-D$^+$ energy at a given level. aug-cc-pVDZ results.

2 Molecular Dynamics Simulations

We analyzed the structural changes of DMP upon ionization to DMP^+ in all obtained AIMD trajectories (see Computational Details in main text). DMP^+ rapidly undergoes structural conversion to DMP-D^+ within the first 100 to 200 fs of simulation time, regardless of the choice of the trajectory snapshot at which the ionization was applied. Subsequently, the cation exhibits molecular vibrations around this equilibrium structure but never transforms into a DMP-L^+ structure. This behavior is illustrated for two trajectories in Figure S8 by means of the two C-N-C-C dihedral angles. The zero in time corresponds to the point at which the ionization DMP $\rightarrow$ DMP^+ was applied. The time evolution of the dihedrals starts from high values of about 170° from the neutral DMP structure, but quickly approaches oscillations around 90°, which is indicative of the DMP-D^+ structure. The combined distribution functions show the frequency of occurrence for each pair of dihedral angle values. The "tails" in this distribution functions in the right of Figure S8 correspond to the relaxation dynamics immediately after ionization. Clearly, the combination of 111° and 168°, which would correspond to DMP-L^+ and is indicated by purple squares, is not observed.

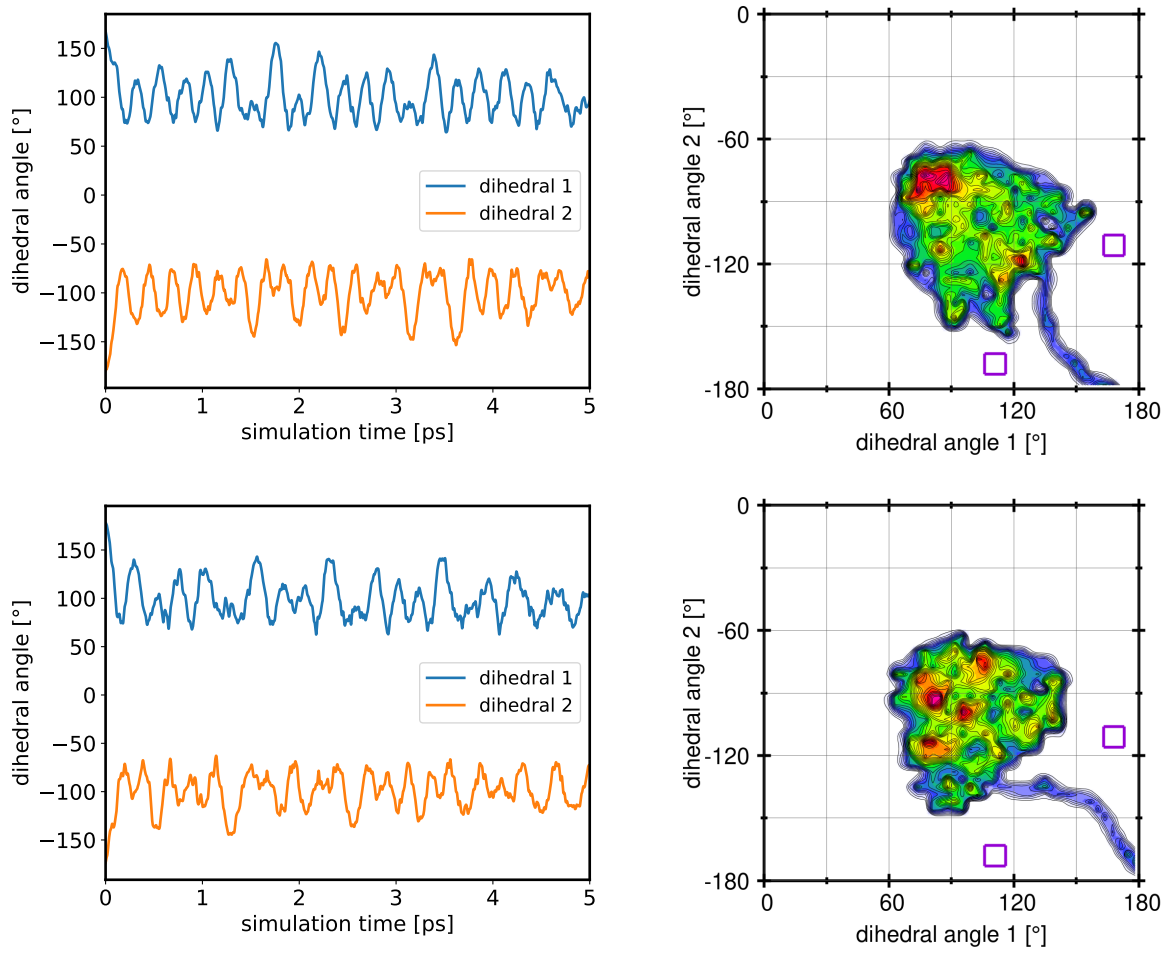

Figure S8: Evolution of the C7-N1-C2-C3 and C8-N4-C5-C6 dihedral angles during simulation time (left) and combined distribution functions[S13,S14] of their simultaneous occurrence (right) for two DMP^+ AIMD trajectories. Dihedrals for DMP-D^+ are 2x $\pm 88°$ and for DMP-L^+ $\pm 111°$ and $\pm 168°$ (purple squares), respectively (sign arbitrary).

3 LR-TDDFT results for stationary points of the Rydberg state

Table S1: Electronic energy differences between DMP-D* and DMP-L* and barrier from the DMP-L* side (in kJ/mol) at different levels using def2-TZVPPD basis sets (aug-cc-pVTZ for SCS-CC2). Structures optimized individually at each level.

method	$\Delta E_{\mathrm{L}\rightarrow\mathrm{D}}$	$\Delta E^{\ddagger}_{\mathrm{L}\rightarrow\mathrm{D}}$
TD-PBE+D3(BJ)	−35.9	1.4
TD-PBE0+D3(BJ)	−35.2	1.2
TD-BHandHLYP+D3(BJ)	−31.9	2.7
TD-ωB97XD	−22.1	8.1
LR-SCS-CC2	−22.8	5.2

4 Structures of the Rydberg State Minima

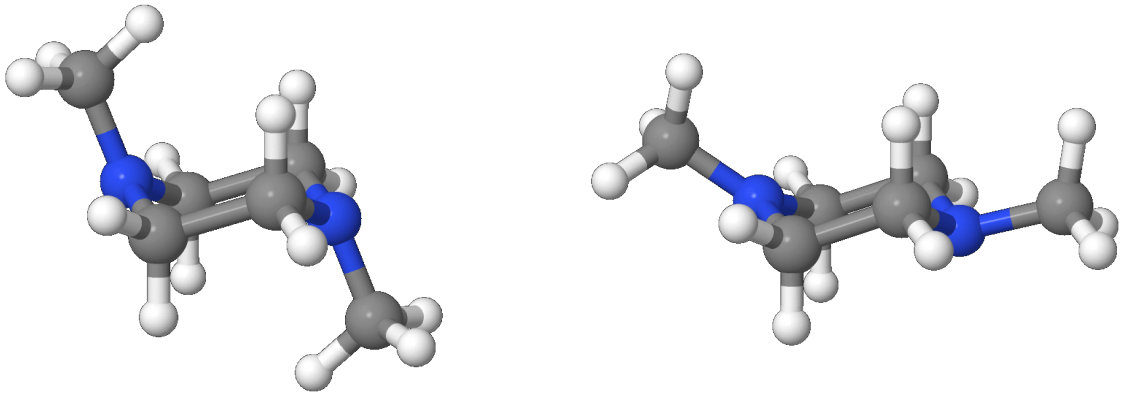

Figure S9: Structures of the two isomers of the Rydberg state of DMP (left: DMP-D*, right: DMP-L*). Structures were optimized at the SCS-CC2/aug-cc-pVTZ level.

References

(S1) Gałyńska, M.; Ásgeirsson, V.; Jónsson, H.; Bjornsson, R. Localized and Delocalized States of a Diamine Cation: Resolution of a Controversy. *J. Phys. Chem. Lett.* **2021**, *12*, 1250–1255.

(S2) Lykos, P.; Pratt, G. W. Discussion on The Hartree-Fock Approximation. *Rev. Mod. Phys.* **1963**, *35*, 496–501.

(S3) Leininger, M. L.; Nielsen, I. M. B.; Crawford, T. D.; Janssen, C. L. A New Diagnostic for Open-Shell Coupled-Cluster Theory. *Chem. Phys. Lett.* **2000**, *328*, 431–436.

(S4) Jiang, W.; DeYonker, N. J.; Wilson, A. K. Multireference Character for 3d Transition-Metal-Containing Molecules. *J. Chem. Theory Comput.* **2012**, *8*, 460–468.

(S5) Chiles, R. A.; Dykstra, C. E. An Electron Pair Operator Approach to Coupled Cluster Wave Functions. Application to He_2, Be_2, and Mg_2 and Comparison with CEPA Methods. *J. Chem. Phys.* **1981**, *74*, 4544–4556.

(S6) Handy, N. C.; Pople, J. A.; Head-Gordon, M.; Raghavachari, K.; Trucks, G. W. Size-Consistent Brueckner Theory Limited to Double Substitutions. *Chem. Phys. Lett.* **1989**, *164*, 185–192.

(S7) Watts, J. D.; Gauss, J.; Bartlett, R. J. Coupled-Cluster Methods with Noniterative Triple Excitations for Restricted Open-Shell Hartree–Fock and Other General Single Determinant Reference Functions. Energies and Analytical Gradients. *J. Chem. Phys.* **1993**, *98*, 8718–8733.

(S8) Stanton, J. F.; Gauss, J. Analytic Energy Derivatives for Ionized States Described by the Equation-of-Motion Coupled Cluster Method. *J. Chem. Phys.* **1994**, *101*, 8938–8944.

(S9) Kaldor, U. The Ground State Geometry of the NO_3 Radical. *Chem. Phys. Lett.* **1990**, *166*, 599–601.

(S10) Malmqvist, P. Å. Calculation of Transition Density Matrices by Nonunitary Orbital Transformations. *Int. J. Quantum Chem.* **1986**, *30*, 479–494.

(S11) Thom, A. J. W.; Head-Gordon, M. Hartree–Fock solutions as a quasidiabatic basis for nonorthogonal configuration interaction. *J. Chem. Phys.* **2009**, *131*, 124113.

(S12) Jensen, K. T.; Benson, R. L.; Cardamone, S.; Thom, A. J. W. Modeling Electron Transfers Using Quasidiabatic Hartree–Fock States. *J. Chem. Theory Comput.* **2018**, *14*, 4629–4639.

(S13) Brehm, M.; Kirchner, B. TRAVIS - A Free Analyzer and Visualizer for Monte Carlo and Molecular Dynamics Trajectories. *J. Chem. Inf. Model.* **2011**, *51*, 2007–2023.

(S14) Brehm, M.; Thomas, M.; Gehrke, S.; Kirchner, B. TRAVIS - A Free Analyzer for Trajectories from Molecular Simulation. *J. Chem. Phys.* **2020**, *152*, 164105.